buildings

Article

Experimental and Analytical Investigation of Bond Behavior of Deformed Steel Bar and Ultra-High Performance Concrete

Rui Liang [1,2], Yuan Huang [1,3,*] and Zhenming Xu [1]

1 College of Civil Engineering, Hunan University, Changsha 410082, China; liangrui33@hnu.edu.cn (R.L.); xuzhenming@hnu.edu.cn (Z.X.)
2 School of Civil Engineering and Architecture, Xinjiang University, Urumqi 830000, China
3 Hunan Provincial Key Laboratory on Damage Diagnosis for Engineering Structures, College of Civil Engineering, Hunan University, Changsha 410082, China
* Correspondence: huangy@hnu.edu.cn

Abstract: Ultra-high performance concrete (UHPC) has been demonstrated to be a realistic alternative to less maintenance and significantly longer service life due to its better mechanical properties and low permeability. The bond performance of the deformed steel bar embedded in UHPC is critically important for the safety of the UHPC structures. This paper conducted an experimental investigation on the bond behavior of deformed steel bars and UHPC. The impacts of loading method, UHPC strength, steel fiber type and content, rebar diameter, and cover thickness were studied. The testing results revealed that the specimens failed in three modes: pull-out, splitting + pull-out, and cone failure. The main factors affecting the bond strength are UHPC compressive strength, cover thickness, and fiber characteristics. The peak slip of rebar-UHPC increases with cover thickness and rebar diameter. Finally, an analytical model of the bond stress-slip relationship between the UHPC and deformed steel bar is obtained, which is in suitable agreement with the test results.

Keywords: ultra-high performance concrete; deformed steel bar; bond-slip; experimental investigation; analytical study; bond toughness

Citation: Liang, R.; Huang, Y.; Xu, Z. Experimental and Analytical Investigation of Bond Behavior of Deformed Steel Bar and Ultra-High Performance Concrete. *Buildings* **2022**, *12*, 460. https://doi.org/10.3390/buildings12040460

Academic Editor: Jorge de Brito

Received: 23 February 2022
Accepted: 30 March 2022
Published: 8 April 2022

1. Introduction

Ultra-high performance concrete (UHPC) has ultra-high strength, toughness, and excellent durability [1], which is suitable for new construction, structural strengthening [2], and restoration projects such as high-rise buildings, long-span bridges [3], and ultra-thin building components [4,5]. The excellent impermeability and very high density of UHPC prevent the penetration of corrosive substances [6], providing better corrosion protection for steel reinforcement, extending the service life of concrete structures, and reducing maintenance costs [7]. With the development of precast concrete structures, UHPC is widely used in joints to improve the overall performance of the structures [8,9]. The bond property between rebar and UHPC is the premise of the two materials working together. It also has an essential influence on the structural load-bearing capacity, stiffness, and crack control.

Compared with normal-strength concrete and fiber reinforced concrete, the particular material properties of UHPC will inevitably lead to changes in the bond property between rebar and UHPC [10]. First of all, the UHPC component does not contain coarse aggregate, and the optimized particle gradation makes it have a compact internal structure. The interface with the rebar is contacted more closely, and the chemical bonding force between the two is enhanced. Secondly, the mechanical interlocking between rebar and UHPC is improved due to the material's ultra-high compressive strength and elastic modulus. Finally, steel fibers in the UHPC restraint the crack development. When the steel fiber content reaches 1.5–2%, the UHPC shows strain hardening characteristics [11], which positively improves the mechanical interlocking and friction between the rebar and UHPC.

Bond strength and peak slip are the key parameters to study the bond behavior between rebar and UHPC. Fehling et al. [12] conducted a pull-out test on rebars with a diameter of 12 mm. They found that increasing the cover thickness would increase the bond strength of UHPC and discussed the influence of cover thickness on the bond failure mode. Yoo et al. [11] concluded that the compressive strength of UHPC was the critical factor determining the bond strength. Marchand et al. [13] studied the bond performance of rebar embedded in UHPC through monotonic and cyclic loading. They proposed a bond strength formula considering two main factors: compressive strength and cover thickness. Alkaysi et al. [14] found that when the fiber content changed from 1 to 2%, the bond strength increased by 36%. Sturm and Visintin [15] concluded that the bond property was insensitive to the types of the steel fiber, and the main factors were the compressive strength and the cover thickness. Hu et al. [16] showed that the rebar-UHPC bond strength only increased by 0.2% when the fiber volume content varied from 1 to 3%. In the existing studies on rebar-UHPC bond strength, there are no unified conclusions on the influence of fiber content, and there are few studies concerning the effect of fiber type on bond strength.

The bond strength will be affected by the diameter of the rebar, which is the "size effect" in bond performance [17–21]. Kook et al. [22] concluded that the bond strength of rebar-UHPC could be effectively improved by increasing the strength grade of rebar, while the bond strength decreased with the increase in rebar diameter (16–22 mm). Lagier et al. [23] conducted direct tension pull-out tests on specimens with large-diameter rebars (25 and 35 mm) and UHPC. They concluded that there was no noticeable size effect on bond strength. Most of the previous research on the bond performance of rebar-UHPC did not consider the size effect. Previous tests [16,24–26] provide a limited amount of data. Because the size of the specimen is not proportional to the diameter of the steel bar, these tests cannot clearly show the size effect.

The peak slip s_u has an essential effect on the stiffness of the rising segment of the bond-slip curve. Existing studies have shown that concrete compressive strength, cover thickness, stirrup, fiber content and type, rebar diameter, and rib spacing affect the peak slip [27]. Therefore, Murcia-Delso et al. [28] suggested determining the peak slip through specific tests. Still, it should be estimated through an empirical formula when the test data cannot be obtained. Based on the bond test between rebar and HPFRCC, Chao et al. [29] concluded that the peak slip was directly proportional to the peak bond stress but inversely proportional to the matrix material's compressive strength and rebar diameter. Sturm and Visintin [15] conducted the pull-out test of UHPFRC. They found that the fiber content had no effect on the peak slip, and s_u was closely related to the cover thickness and compressive strength. Wu and Zhao [30] concluded that the peak slip is mainly related to the cover thickness and stirrup content through regression analysis of normal-strength reinforced concrete data. Xu [31] believed that the peak slip was associated with the rebar diameter based on many pull-out tests. Murcia-Delso et al. [28] found that the peak slip is related to the rebar diameter, which is about $0.07d_b$, through the bond test of large-diameter rebars (36, 43, and 57 mm). Zhao and Zhu [32] proposed that the peak slip s_u is $0.07442d_b$–$0.00093{d_b}^2$. At present, most studies on the peak slip of rebars are focused on normal-strength concrete. Therefore, the survey on the peak slip of rebar-UHPC needs to be carried out.

Local bond-slip relationships significantly influence the bearing capacity, stiffness, and deformation capacity of reinforced concrete structures [27,30,33]. The bond stress-slip constitutive model is obtained based on the regression analysis of many test data. However, the bond stress-slip curves are also quite different due to the complex bonding mechanism and differences in test conditions [34–40]. According to the author's knowledge, Marchand [13], Yoo [11], and Sturm and Visintin [15] studied the bond-slip relationship between rebar and UHPC. Zhou [41] analyzed the bond-slip behavior of epoxy-coated rebar embedded in UHPC. Marchand [13] and Yoo [11] proposed an ascending section of the bond-slip relationship between rebar and UHPC. Due to the discreteness of test data, the proposed bond-slip constitutive model did not discuss the descending branch. Sturm and Visintin [15] proposed two types of bond-slip models for pull-out and splitting failure modes, respectively. In conclusion, the descending branch of the bond-slip models for UHPC is unclear and needs to be investigated [41].

This study aims to conduct pull-out tests to provide the bond properties of deformed rebars in UHPC. Considering the influence of compressive strength, fiber content, fiber type, cover thickness, rebar diameter, and rebar yield strength, we quantified the bond strength and peak slip for deformed rebars in UHPC. We also compared the influence of the loading method on the bond property. In addition, we proposed the local bond stress-slip constitutive model of rebar in UHPC.

2. Experimental Program

2.1. Specimen Details

A total of 69 pull-out specimens were tested in this research. The range of design variables and details of the specimens were listed in Tables 1 and 2, respectively. The bond length was twice the rebar diameter to ensure the pull-out failure and obtain a relatively uniformly distributed bond stress [11,15]. The specimen geometry is shown in Figure 1. A PVC pipe at the loading end debonds the rebar from UHPC to avoid local failure.

Table 1. Range of design variables.

Design Variables	Variation Range
Compressive strength f_c	UA, UB, UC, UD
Fiber volume content V_f	1%, 2%, 3%
Fiber type	SFA, SFB, SFC, HFB
Cover thickness c	$1d_b$, $2d_b$, $3d_b$, $4d_b$, $5.75d_b$
Rebar diameter d_b	12 mm, 16 mm, 20 mm, 25 mm
Rebar yield strength f_y	422 MPa, 542 MPa, 680 MPa
Loading method	P, RP
Debonded length (The distance between the bonded part and the specimen loading surface)	0, $2.5d_b$, $5.25d_b$

Note: UA: compressive strength of UHPC at 3 days cure time; UB: compressive strength of UHPC at 7 days cure time; UC: compressive strength of UHPC at 14 days cure time; UD: compressive strength of UHPC at 28 days cure time. SFA: straight steel fiber with an aspect ratio of 30; SFB: straight steel fiber with an aspect ratio of 65; SFC: straight steel fiber with an aspect ratio of 100; HFB: hooked steel fiber with an aspect ratio of 65. P: traditional pull-out test; RP: revised pull-out test.

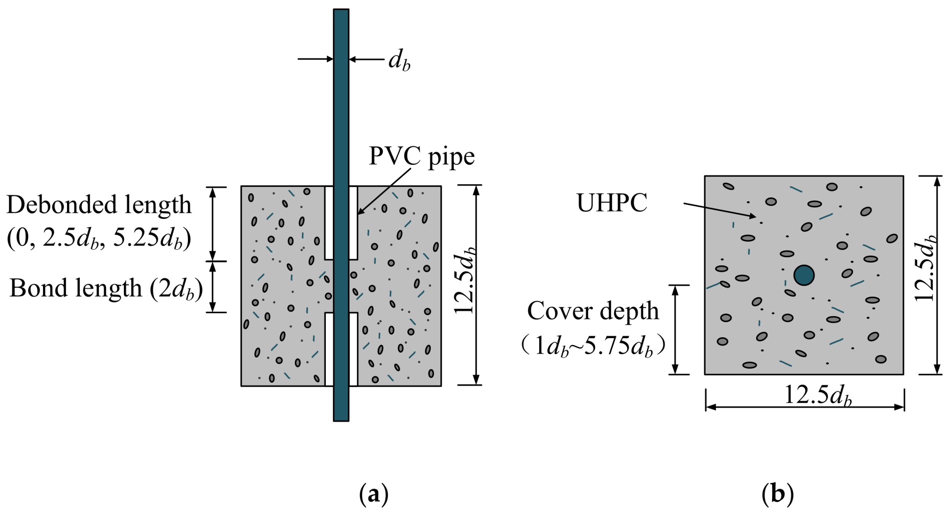

Figure 1. Dimension of specimens: (**a**) profile view; (**b**) plan view.

Table 2. Details of specimens.

Test Variable	Specimen	f_c (MPa)	f_t (MPa)	c (mm)	d_b (mm)	V_f (%)	Fiber Type	Loading Method	Debonded Length (mm)	Rebar Yield Strength (MPa)
Control group	UD-S02B-6D16C5-P5	139.82	9.38	92	16	2	SFB	Pull-out	84	680
Compressive strength	UA-S02B-6D16C5-P5	98.34	6.86	92	16	2	SFB	Pull-out	84	680
	UB-S02B-6D16C5-P5	109.64	7.24	92	16	2	SFB	Pull-out	84	680
	UC-S02B-6D16C5-P5	116.10	8.50	92	16	2	SFB	Pull-out	84	680
Fiber volume content	UD-S01B-6D16C5-P5	125.18	8.24	92	16	1	SFB	Pull-out	84	680
	UD-S03B-6D16C5-P5	144.97	9.57	92	16	3	SFB	Pull-out	84	680
Fiber type	UD-S02A-6D16C5-P5	129.93	8.27	92	16	2	SFA	Pull-out	84	680
	UD-S02C-6D16C5-P5	141.89	9.72	92	16	2	SFC	Pull-out	84	680
	UD-H02B-6D16C5-P5	133.82	9.05	92	16	2	HFB	Pull-out	84	680
Cover thickness	UD-S02B-6D16C1-P5	139.82	9.38	16	16	2	SFB	Pull-out	84	680
	UD-S02B-6D16C2-P5	139.82	9.38	32	16	2	SFB	Pull-out	84	680
	UD-S02B-6D16C3-P5	139.82	9.38	48	16	2	SFB	Pull-out	84	680
	UD-S02B-6D16C4-P5	139.82	9.38	64	16	2	SFB	Pull-out	84	680
Rebar diameter	UD-S02B-5D12C5-P5	139.82	9.38	92	12	2	SFB	Pull-out	84	520
	UD-S02B-5D16C5-P5	139.82	9.38	92	16	2	SFB	Pull-out	84	542
	UD-S02B-5D20C5-P5	139.82	9.38	92	20	2	SFB	Pull-out	84	539
	UD-S02B-5D25C5-P5	139.82	9.38	92	25	2	SFB	Pull-out	84	534
Rebar yield strength	UD-S02B-4D16C5-P5	139.82	9.38	92	16	2	SFB	Pull-out	84	422
Loading method and debonded length	UD-S02B-6D16C5-P0	139.82	9.38	92	16	2	SFB	Pull-out	0	680
	UD-S02B-6D16C5-P2.5	139.82	9.38	92	16	2	SFB	Pull-out	40	680
	UD-S02B-6D16C5-RP0	139.82	9.38	92	16	2	SFB	Revised pull-out	0	680
	UD-S02B-6D16C5-RP2.5	139.82	9.38	92	16	2	SFB	Revised pull-out	40	680
	UD-S02B-6D16C5-RP5	139.82	9.38	92	16	2	SFB	Revised pull-out	84	680

Note: f_c: compressive strength of concrete cubes; f_t: tensile strength of dog-bone specimens. The reported strength values are the average of the measurements of three nominally identical specimens.

All test parameters and specimen numbers are shown in Table 2.

The specimens are numbered according to the tested parameters. For example, UD-S02B-6D16C5-P5: UD represents the compressive strength of the UHPC curing period of 28 days. In S02B, S represents straight steel fiber, 02 represents fiber volume content of 2%. B represents the aspect ratio of 65. 6 in 6D16C5 means that the rebar yield strength is 680 MPa, D16 means that the rebar diameter is 16 mm, and C5 means that the cover thickness is 5.75 times the diameter of the rebar. P5 represents the traditional pull-out test, and the debonded length is 84 mm ($5.25d_b$).

According to GB/T 31387-2015 [42], the UHPC compressive strength was tested from a cubic block with a side length of 100 mm. The UHPC tensile strength was obtained from the dog-bone specimen shown in Figure 2b. The UHPC compressive and tensile strength are listed in Table 2.

(a) (b)

Figure 2. Test setup for UHPC mechanical properties: (**a**) compressive test; (**b**) direct tension test.

Each result is the mean of three specimens. The first half of Table 2 (up to UD-H02B-6D16C5-P5) contains the test variables of compressive strength, fiber volume content, and fiber type related to the UHPC properties. Therefore, the UHPC compression and tensile strength results are different for these groups. The UHPC properties of the other test groups, including cover thickness, rebar diameter, rebar yield strength, loading method, and debonded length, were identical.

2.2. Materials Properties

The mix proportion design of UHPC is listed in Table 3. To improve the workability of the mixture, we used a polycarboxylic acid superplasticizer [43].

Table 3. Mix proportion design of UHPC (mass/cement mass ratio) [43].

Cement	Quartz Sand	Silica Flour	Silica Fume	Fly Ash	Water/Binder Ratio
1.0	1.1	0.3	0.25	0.1	0.18

Note: Steel fiber is 1~3% by volume fraction. Superplasticizer is 0.2% of binder by mass.

Four kinds of brass-coated steel fibers were used in the experiment (Hunan Guli Engineering New Materials Co., Ltd., Changsha, China), including three straight steel fibers and one hooked steel fiber. The straight steel fibers have different aspect ratios, which were identified as steel fiber A (SFA), steel fiber B (SFB), steel fiber C (SFC). The hooked steel fiber B was numbered as HFB. The steel fibers are pictured in Figure 3 (length of the fiber, L_f; diameter of the fiber, d_f). The fiber characteristic parameters are listed in Table 4.

(a) (b) (c) (d)

Figure 3. Different types of steel fibers: (**a**) SFA; (**b**) SFB; (**c**) SFC; (**d**) HFB.

Table 4. Properties of high-strength steel fibers.

Steel Fiber ID	Form	L_f (mm)	d_f (mm)	L_f/d_f	Tensile Strength (MPa)
SFA	Straight	6	0.2	30	≥2850
SFB	Straight	13	0.2	65	≥2850
SFC	Straight	20	0.2	100	≥2850
HFB	Hooked	13	0.2	65	≥2850

Note: L_f: length of the fiber; d_f: diameter of the fiber.

Hot-rolled deformed steel bars (HRB) were used in the pull-out test. Rebar grades HRB400, HRB500, and HRB600 were used based on GB/T 1499.2-2018 [44]. The surface shape of the deformed rebar is shown in Figure 4. Table 5 summarizes the mechanical properties and geometric characteristics of the rebar.

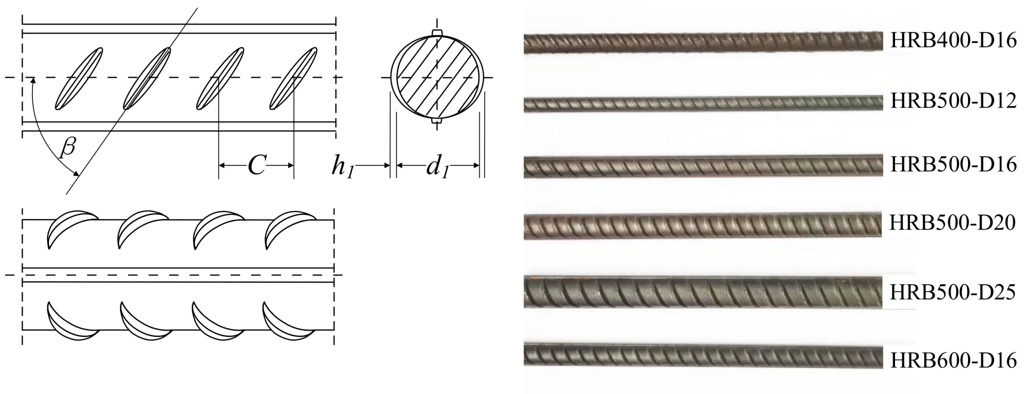

(**a**) (**b**)

Figure 4. The surface configuration of deformed bars: (**a**) schematic diagram; (**b**) photo of deformed bars.

Table 5. Geometric and mechanical properties of steel bars.

Type of Steel Bars	HRB400-D16	HRB500-D12	HRB500-D16	HRB500-D20	HRB500-D25	HRB600-D16
Nominal diameter d_b (mm)	16	12	16	20	25	16
Core diameter d_1 (mm)	15.4	11.5	15.4	19.3	24.2	15.4
Average rib depth h_1 (mm)	1.5	1.0	1.5	1.7	2.0	1.5
Rib inclination β (°)	60.5	60	60.5	65.2	76.3	60.5
Rib spacing C (mm)	10	7.9	10.0	11.0	12.5	10
Yield strength f_y (MPa)	422	520	542	539	534	680
Ultimate strength f_u (MPa)	583	695	716	714	708	861

2.3. Test Setup and Loading Scheme

Two experimental setups were used in the study, namely the traditional pull-out setup and the revised pull-out test setup. The traditional pull-out test in Figure 5a [45] was used to investigate the effect of various factors on the bond performance of rebar-UHPC in this paper. A 20 mm-thick steel plate and a 5 mm-thick rubber plate were placed between the hydraulic jack and the specimen. The surrounding concrete behind the rubber plate forms compression struts while loading [46]. The revised pull-out test is shown in Figure 5b. A steel bracket was placed on the specimen to eliminate the compression strut reaction of the concrete. Both the rebar and the surrounding UHPC were in tension [14]. By changing the distance from the reinforcement bonded part to the loading end, namely the debonded length, the effects of the two loading methods on the bond performance of the rebar-UHPC interface were compared. Strain gauges were attached to the reinforcing bars near the loading end to monitor steel yielding. Two linear displacement transducers (LVDTs) were arranged at the free end of the specimen to measure the relative slip between the rebar and UHPC.

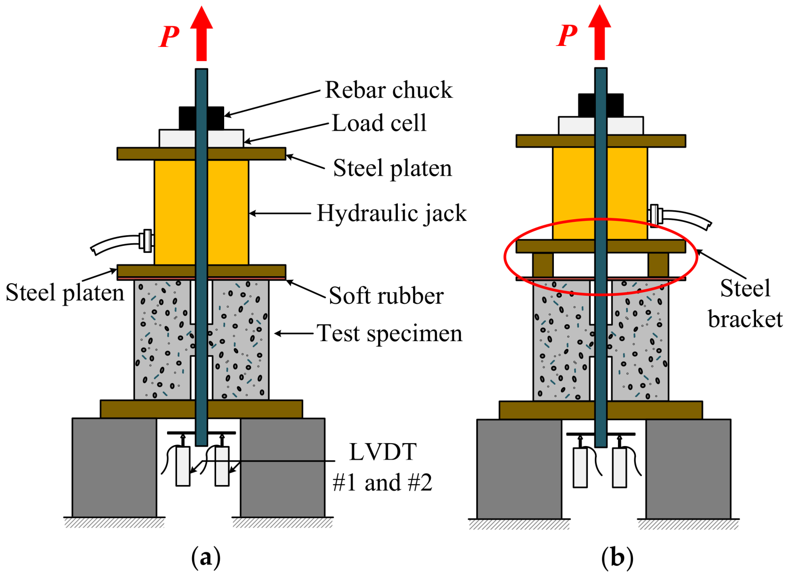

Figure 5. Pull-out test setup: (**a**) traditional pull-out; (**b**) revised pull-out.

The tensile load was applied with a step of 2 kN until ultimate load, then a displacement load of 0.2 mm was applied per level until the slip reached 20 mm.

3. Results and Discussion

3.1. Bond Capacity Parameters

The average bond stress between the rebar and the UHPC interface was calculated as follows:

$$\tau = \frac{F}{\pi d_b l_d} \tag{1}$$

where τ is the average bond stress, F is the axial pull-out load, d_b is the rebar diameter, and l_d is the bond length.

The relative slip s of the steel bar and UHPC interface was obtained as follows:

$$s = \frac{s_1 + s_2}{2} \tag{2}$$

where s_1 and s_2 are the slip measured by LVDT#1 and LVDT#2, respectively. Free end slip was measured to eliminate the effect of elastic deformation of the reinforcement.

Bond toughness is a measure of energy dissipation in the process of bond-slip, which was calculated as the area under the bond-slip curve corresponding to the target slip as follows:

$$A_i = \int_0^{s_i} \tau ds \tag{3}$$

where s_i is the target slip, selected as the peak slip, and the slips corresponding to 80% and 50% of the post-peak bond stress.

The peak bond stress τ_u, peak slip s_u, peak bond toughness A_p, post-peak bond toughness A_{80} and A_{50} mean the areas under the bond stress-slip curves when post-peak stress drops to 80% and 50% of the peak bond stress, respectively, are listed in Table 6.

Table 6. Experimental results.

Specimen	τ_u (MPa)	Mean	s_u (mm)	Mean	A_p (MPa.mm)	Mean	A_{80} (MPa.mm)	Mean	A_{50} (MPa.mm)	Mean	Failure Modes
UD-S02B-6D16C5-P5-1	61.36	63.46	0.52	0.56	23.39	29.45	141.02	138.26	238.40	240.72	PO
UD-S02B-6D16C5-P5-2	61.72		0.61		34.58		143.09		257.13		PO
UD-S02B-6D16C5-P5-3	67.31		0.54		30.37		130.66		226.65		PO
UA-S02B-6D16C5-P5-1	52.72	50.45	0.55	0.53	20.63	23.08	109.46	100.47	214.63	192.66	PO
UA-S02B-6D16C5-P5-2	51.17		0.42		19.43		89.54		183.30		PO
UA-S02B-6D16C5-P5-3	47.44		0.61		29.19		102.41		180.04		PO
UB-S02B-6D16C5-P5-1	60.82	57.21	0.57	0.56	29.29	27.07	122.92	131.42	213.38	236.70	PO
UB-S02B-6D16C5-P5-2	59.61		0.53		27.56		131.70		244.02		PO
UB-S02B-6D16C5-P5-3	51.20		0.57		24.37		139.63		252.70		PO
UC-S02B-6D16C5-P5-1	60.24	61.12	0.55	0.54	28.12	27.71	129.25	132.21	212.37	231.20	PO
UC-S02B-6D16C5-P5-2	64.80		0.53		27.39		128.37		230.00		PO
UC-S02B-6D16C5-P5-3	58.31		0.53		27.63		139.01		251.23		PO
UD-S01B-6D16C5-P5-1	59.48	58.45	0.60	0.56	32.86	29.07	135.03	138.05	223.88	229.08	PO
UD-S01B-6D16C5-P5-2	58.18		0.47		23.36		148.28		249.11		PO
UD-S01B-6D16C5-P5-3	57.69		0.62		30.99		130.85		214.24		PO
UD-S03B-6D16C5-P5-1	74.57	71.71	0.58	0.55	38.48	34.25	149.06	141.09	294.69	273.54	PO
UD-S03B-6D16C5-P5-2	67.92		0.48		26.18		143.51		274.47		PO
UD-S03B-6D16C5-P5-3	72.63		0.60		38.09		130.70		251.46		PO
UD-S02A-6D16C5-P5-1	60.37	58.00	0.56	0.58	27.46	28.82	135.71	136.43	226.62	220.71	PO
UD-S02A-6D16C5-P5-2	58.85		0.68		35.87		127.27		202.79		PO
UD-S02A-6D16C5-P5-3	54.78		0.49		23.13		146.29		232.73		PO
UD-S02C-6D16C5-P5-1	63.23	66.97	0.58	0.57	33.67	30.48	142.19	142.54	245.16	264.08	PO
UD-S02C-6D16C5-P5-2	67.67		0.50		23.52		139.04		261.71		PO
UD-S02C-6D16C5-P5-3	70.00		0.62		34.25		146.38		285.38		PO
UD-H02B-6D16C5-P5-1	62.74	63.47	0.64	0.51	34.80	27.98	138.50	133.05	283.90	258.65	PO
UD-H02B-6D16C5-P5-2	63.33		0.46		25.62		129.01		243.27		PO
UD-H02B-6D16C5-P5-3	64.35		0.42		23.51		131.64		248.78		PO
UD-S02B-6D16C1-P5-1	49.63	50.32	0.40	0.39	17.29	17.01	102.03	94.02	194.66	179.02	PO
UD-S02B-6D16C1-P5-2	54.46		0.43		19.42		85.17		157.38		PO
UD-S02B-6D16C1-P5-3	46.86		0.35		14.31		94.85		185.02		PO
UD-S02B-6D16C2-P5-1	59.79	59.16	0.40	0.44	20.55	22.61	98.98	109.40	187.73	197.50	PO
UD-S02B-6D16C2-P5-2	58.54		0.48		23.67		121.03		204.28		PO
UD-S02B-6D16C2-P5-3	59.14		0.43		23.61		108.20		200.50		PO
UD-S02B-6D16C3-P5-1	60.15	60.73	0.39	0.46	20.09	22.94	120.69	112.88	210.43	206.13	PO
UD-S02B-6D16C3-P5-2	61.36		0.43		20.71		106.01		216.18		PO
UD-S02B-6D16C3-P5-3	60.68		0.55		28.01		111.95		191.77		PO
UD-S02B-6D16C4-P5-1	62.66	63.16	0.45	0.52	22.39	28.72	107.15	115.87	225.69	218.61	PO
UD-S02B-6D16C4-P5-2	67.71		0.60		36.54		128.52		216.01		PO
UD-S02B-6D16C4-P5-3	59.12		0.50		27.22		111.92		214.11		PO
UD-S02B-5D12C5-P5-1	62.85	59.59	0.48	0.51	21.10	23.26	123.47	128.19	204.27	216.46	PO
UD-S02B-5D12C5-P5-2	60.54		0.56		29.48		126.43		226.02		PO
UD-S02B-5D12C5-P5-3	55.38		0.48		19.20		134.68		219.10		PO
UD-S02B-5D16C5-P5-1	59.42	60.42	0.54	0.54	26.16	27.16	135.51	137.82	268.31	270.49	PO
UD-S02B-5D16C5-P5-2	58.51		0.54		26.43		130.40		262.15		PO
UD-S02B-5D16C5-P5-3	63.33		0.55		28.88		147.54		281.00		PO
UD-S02B-5D20C5-P5-1	59.78	58.02	1.31	1.32	70.97	70.28	253.84	256.72	394.06	399.93	PO
UD-S02B-5D20C5-P5-2	57.25		1.34		69.70		261.77		404.21		PO
UD-S02B-5D20C5-P5-3	57.02		1.31		70.18		254.56		401.52		PO
UD-S02B-5D25C5-P5-1	56.06	59.31	1.80	1.92	96.62	103.04	286.18	276.36	478.71	458.97	PO
UD-S02B-5D25C5-P5-2	60.41		1.98		103.95		269.87		441.41		PO
UD-S02B-5D25C5-P5-3	61.46		2.00		108.55		273.02		456.78		PO
UD-S02B-4D16C5-P5-1	57.78	56.85	0.52	0.54	24.71	25.35	165.72	167.97	295.26	293.59	PO
UD-S02B-4D16C5-P5-2	55.58		0.65		30.65		162.79		277.03		PO
UD-S02B-4D16C5-P5-3	57.19		0.44		20.69		175.39		308.49		PO
UD-S02B-6D16C5-P0-1	45.04	43.95	0.47	0.47	15.30	15.78	33.14	44.36	62.03	79.73	SP + PO
UD-S02B-6D16C5-P0-2	47.73		0.43		16.48		57.12		99.32		SP + PO
UD-S02B-6D16C5-P0-3	39.07		0.52		15.57		42.83		77.86		SP + PO
UD-S02B-6D16C5-P2.5-1	54.10	57.40	0.61	0.51	21.54	24.30	94.49	105.60	170.10	186.90	PO
UD-S02B-6D16C5-P2.5-2	57.37		0.48		27.47		115.83		208.87		PO
UD-S02B-6D16C5-P2.5-3	60.72		0.43		23.91		106.47		181.73		PO
UD-S02B-6D16C5-RP0-1	36.88	33.91	0.44	0.45	13.15	12.77	49.55	39.65	92.41	77.04	Cone
UD-S02B-6D16C5-RP0-2	32.26		0.52		14.30		40.67		73.01		Cone
UD-S02B-6D16C5-RP0-3	32.58		0.40		10.86		28.73		65.70		Cone
UD-S02B-6D16C5-RP2.5-1	49.50	54.15	0.55	0.55	25.39	23.78	94.94	94.00	136.41	158.96	PO
UD-S02B-6D16C5-RP2.5-2	55.28		0.57		19.37		86.55		166.65		PO
UD-S02B-6D16C5-RP2.5-3	57.67		0.52		26.58		100.52		173.82		PO
UD-S02B-6D16C5-RP5-1	64.17	63.12	0.44	0.51	22.16	26.62	111.18	123.69	177.08	202.12	PO
UD-S02B-6D16C5-RP5-2	60.73		0.60		30.71		125.76		211.36		PO
UD-S02B-6D16C5-RP5-3	64.45		0.51		27.00		134.13		217.92		PO

Note: PO for pull-out of rebar from the UHPC; SP + PO for combined concrete cover splitting and rebar pull-out; cone for UHPC cone failure.

3.2. Failure Mode

Three prevailing types of bond failure can be observed in Figure 6. There were pull-out failure, splitting + pull-out failure, and concrete cone failure. Because the embedment length is only two times the bar's diameter to prevent a rupture of the rebar before pull-out failure [11], there was no rebar fracture failure in this study. The failure modes of all specimens are listed in Table 6.

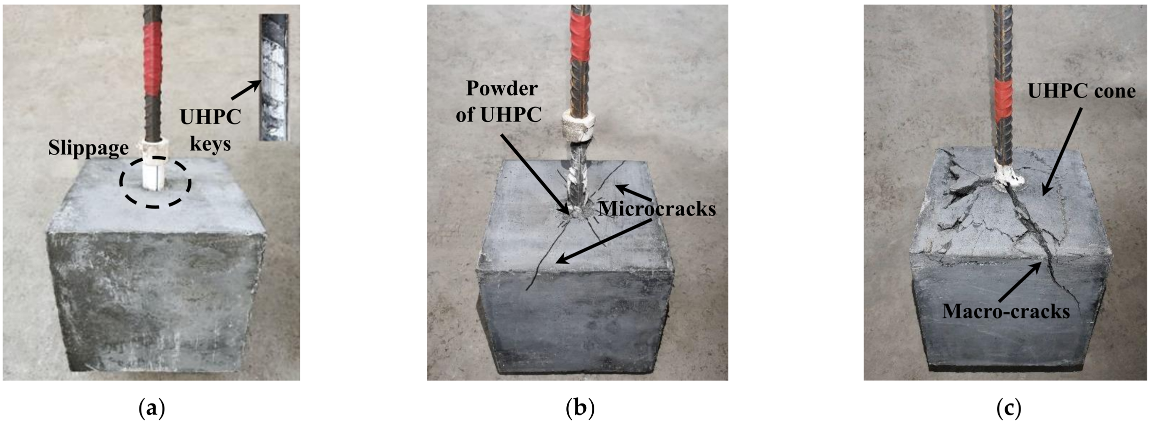

Figure 6. Typical failure modes: (**a**) pull-out failure; (**b**) splitting + pull-out failure; (**c**) cone failure.

For the traditional loading specimens, the ribs of the tensile rebar cut the UHPC around, resulting in pull-out failure. No cracks were observed on the surface of the specimens, as shown in Figure 6a. However, when the bonded part closed to the loading end, radial splitting microcracks were observed on the surface of the specimen near the loading end, resulting in a slip of rebar followed by splitting of UHPC, as shown in Figure 6b. The specimens suffered cone failure, and a significant drop in bond resistance occurred for the revised pull-out specimens when the bonded part was located at the loading end, as shown in Figure 6c.

3.3. Bond Stress-Slip Curves

The bond-slip curves for steel rebar in UHPC are shown in Figure 7, divided into three stages: Firstly, the bond stress is gradually transferred from the loading end to the free end at the beginning of loading. At this stage, all specimens exhibit approximately linear bond-slip behavior. However, its practical application is restricted because this stage is limited compared to the entire bond-slip curve. Secondly, the mechanical interlocking force gradually replaced the chemical bonding force with the load increase. The interface near the loading end generates local debonding, which progresses to the free end, where the UHPC between the steel ribs is further squeezed, and sliding occurs. As a result, the stiffness of the ascending branch diminishes and exhibits nonlinear behavior until the peak load. Finally, the slip increases rapidly with the decrease in the load until the failure of the specimen. The resisting force mainly includes friction rather than aggregate interlocking forces because the UHPC has no coarse aggregate.

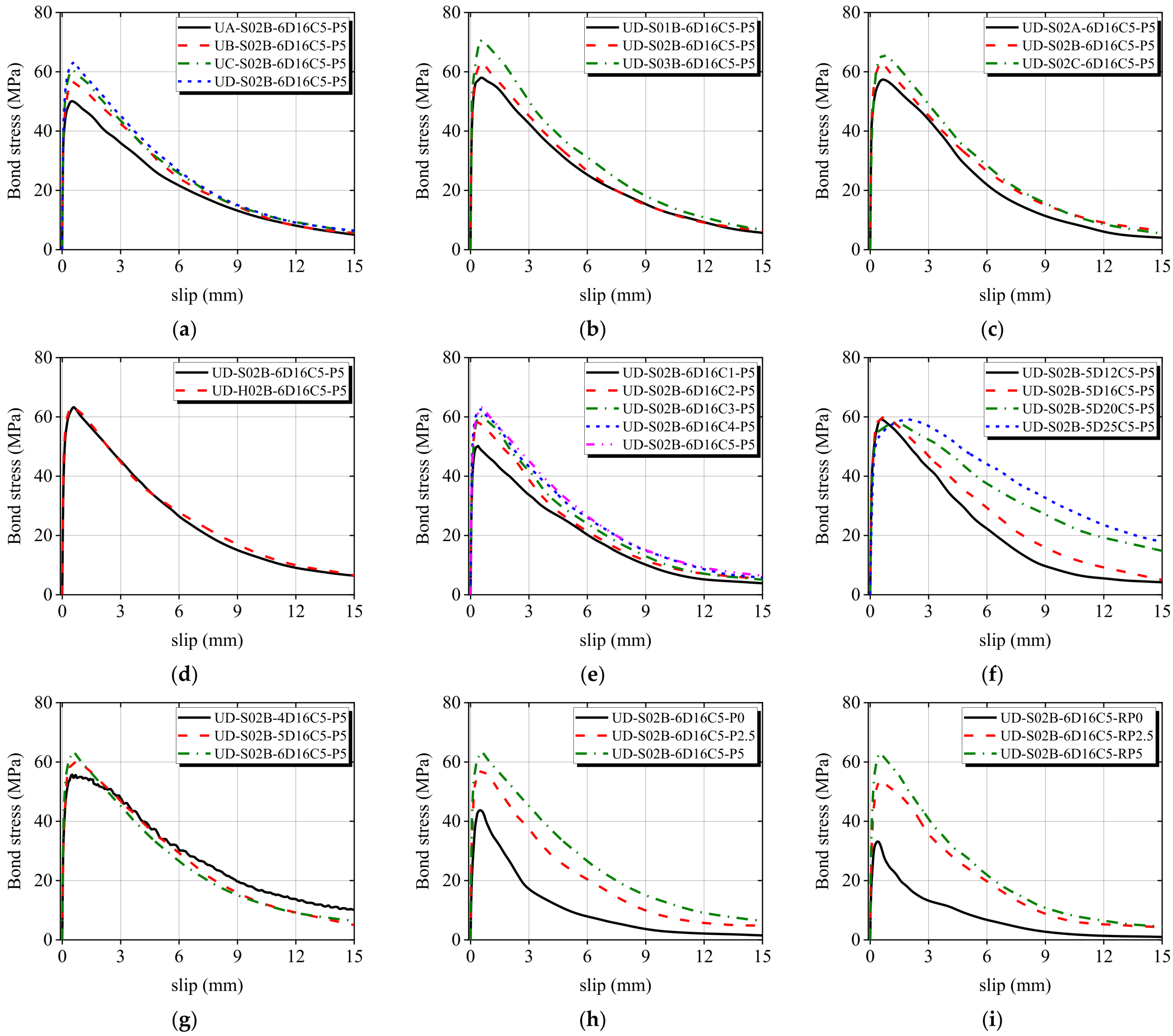

Figure 7. Bond-slip curves of specimens: (**a**) compressive strength; (**b**) fiber volume content; (**c**) fiber aspect ratio; (**d**) fiber type; (**e**) cover thickness; (**f**) rebar diameter; (**g**) rebar yield strength; (**h**) traditional pull-out test; (**i**) revised pull-out test.

3.4. The Effects of Parameters on Bond Behavior

3.4.1. Compressive Strength

The influence of compressive strength on the rebar-UHPC bond property is shown in Figure 8. The most significant factor affecting the bond strength is the concrete compressive strength. The contribution of concrete to bond strength can be described as a power of compressive strength ($f_c^{0.25\sim0.75}$) [35,47]. Based on the test results, an excellent linear correlation between τ_u and $f_c^{0.5}$ (R^2 = 0.99) was obtained, consistent with Alkaysi and El-Tawil's findings [14].

Figure 8b shows that the increase in compressive strength of UHPC improves the bond toughness. When the compressive strength increased from 98.34 to 139.82 MPa, A_p, A_{80}, and A_{50} increased by 27.6%, 37.6%, and 24.9%, respectively.

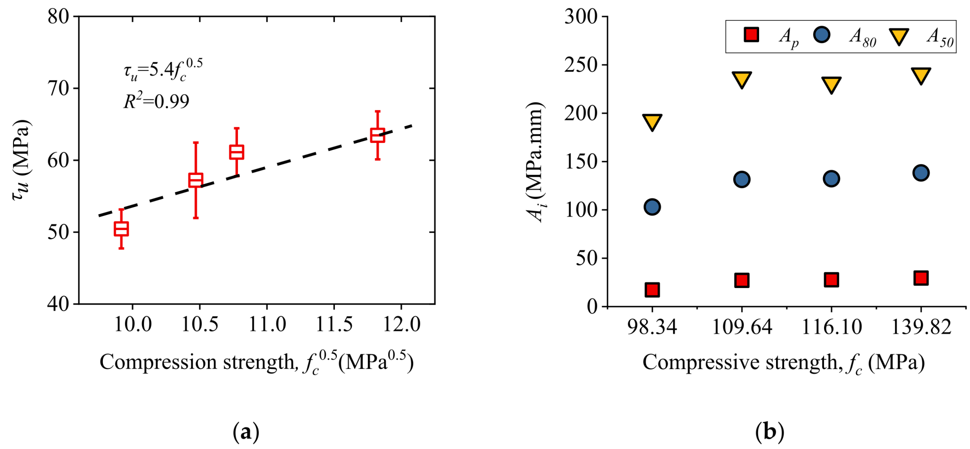

Figure 8. Effect of compressive strength on bond performance: (**a**) bond strength; (**b**) bond toughness.

3.4.2. Steel Fiber

The influence of steel fiber on rebar-UHPC bond property is shown in Figure 9. The increase in fiber volume content can significantly improve the bond strength. When the fiber volume content increased from 1% to 3%, the bond strength increased by 22.7% (Figure 9a). The reason is that the increase in steel fiber can improve the compressive capacity of UHPC and inhibit the microcracks in the specimen to enhance the bond performance [48].

The bond strength also increased with the steel fiber aspect ratio. When the aspect ratio of steel fiber raised from 30 to 100, the bond strength increased by 15.5% (Figure 9b). The bond strength of the specimens with the hook steel fiber has no significant difference from the straight steel fiber.

A fiber characteristic factor λ_f ($\lambda_f = V_f \times L_f/d_f$) was proposed to evaluate the effects of fiber volume content and aspect ratio [49]. The increase in fiber characteristic factors, such as fiber volume content or aspect ratio, can improve fiber bridging effectiveness and, consequently, bond strength [38,50]. The bond strength is plotted against the fiber characteristic factor λ_f in Figure 9c. The bond strength and the fiber characteristic factor have a linear relationship (R^2 = 0.82).

As shown in Figure 9d, with fiber volume content from 1% to 3%, the bond toughness A_P, A_{80}, and A_{50} increased by 17.8%, 2.2%, and 19.4%, respectively. As shown in Figure 9e, the bond toughness A_P, A_{80} were almost unchanged with the fiber aspect ratio. However, A_{50} grew with the fiber aspect ratio. The reason is that the larger fiber aspect ratio plays a more significant role in preventing microcracks.

3.4.3. Cover Thickness

The influence of cover thickness on the bond performance of rebar-UHPC is shown in Figure 10. The pull-out failure occurred in all specimens in the concrete cover group. The bond strength increased by 17.6% when the cover thickness increased from 16 to 32 mm. After that, the bond strength changed little. Marchand et al. [13] concluded that when the cover thickness is greater than $4d_b$, its effect on bond strength can be ignored.

The peak slip raised with the increase in the cover thickness. The peak slip increased by 43.6% when the cover thickness increased from $1d_b$ to $5.75d_b$. Wu and Zhao [30] demonstrated that increasing the cover thickness impacts the ascending branch of the bond-slip curve, resulting in increased peak slip by evaluating a database of plain concrete. The rise of A_p, A_{80}, and A_{50} is 73.1%, 47.1%, and 34.5%, respectively, when the cover thickness increased from $1d_b$ to $5.75d_b$. The reason is that increasing the cover thickness eliminates circumferential tensile stresses on the concrete surface, prevents the development of microcracks inside the specimen [51], and delays the premature concrete cracking, consequently improving the bond performance of the rebar-UHPC interface.

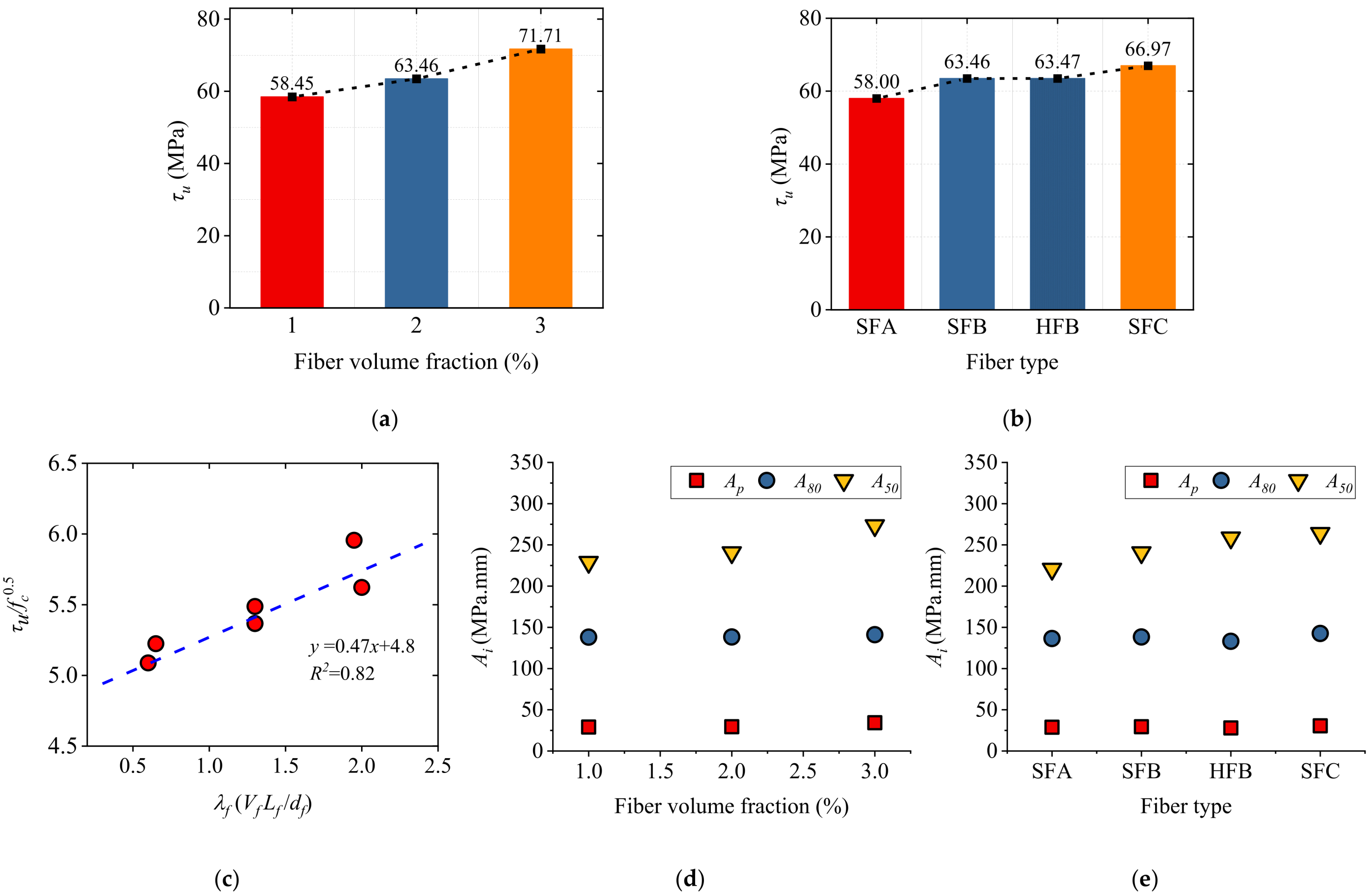

Figure 9. Effect of steel fiber on bond performance: (**a**) bond strength-fiber volume fraction; (**b**) bond strength-fiber type; (**c**) bond strength-fiber characteristic factor; (**d**) bond toughness-fiber volume fraction; (**e**) bond toughness-fiber type.

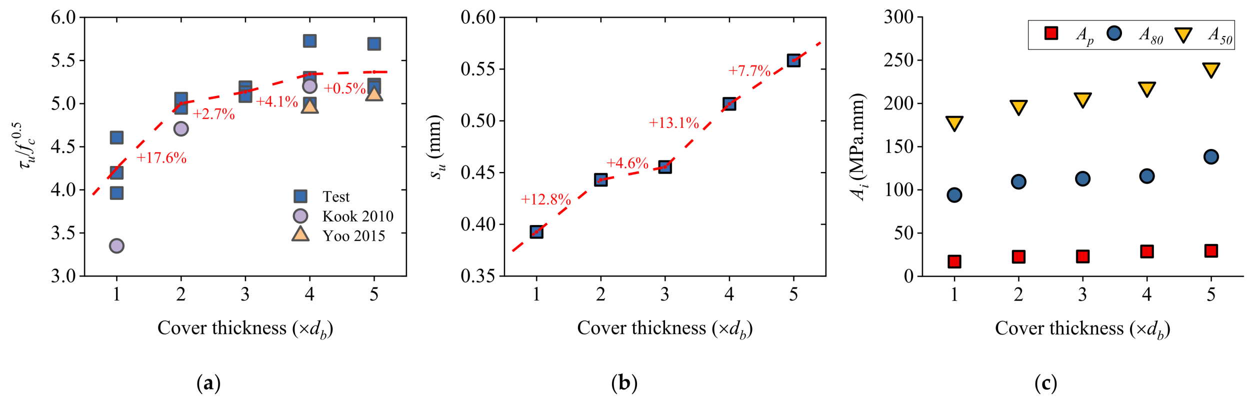

Figure 10. Effect of cover thickness on bond performance: (**a**) bond strength; (**b**) peak slip; (**c**) bond toughness.

3.4.4. Rebar Diameter

The influence of rebar diameter on the bond performance is shown in Figure 11. The bond strength remained almost unchanged with the rebar diameter, indicating that the size effect of rebar on bond strength was negligible.

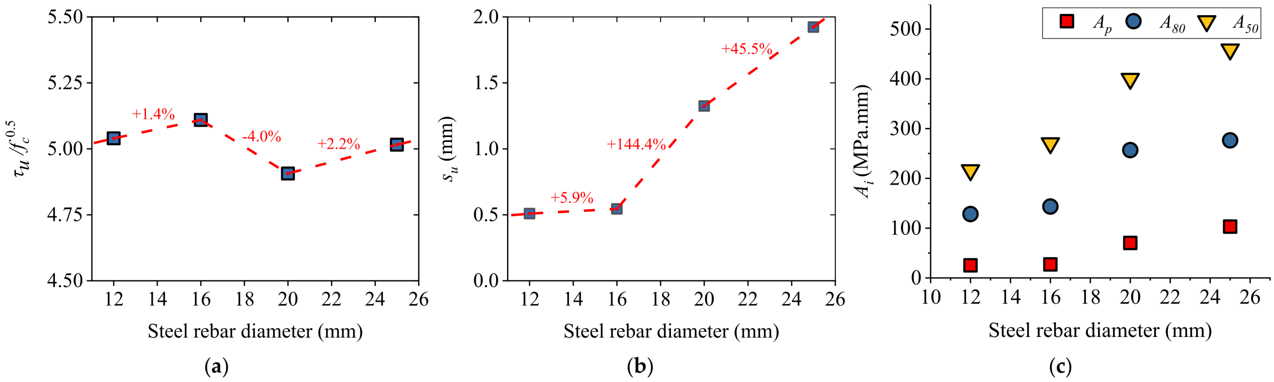

Figure 11. Effect of rebar diameter on bond performance: (**a**) bond strength; (**b**) peak slip; (**c**) bond toughness.

The peak slip increased with the rebar diameter. When the rebar diameter increased from 12 to 25 mm, the peak slip increased by 276.4%. The bond toughness also increased significantly with the rise of the rebar diameter. The A_p, $A_{80,}$ and A_{50} of the specimen with 25 mm rebar were 342.9%, 115.6%, and 112.0% higher than the 12 mm rebar, respectively.

3.4.5. Rebar Yield Strength

The influence of the rebar yield strength on the bond behavior is shown in Figure 12. The bond strength increased with the rebar yield strength, and the HRB400 (f_y = 422 MPa) reinforcement has reached the yield stage. When the rebar yield strength increased from 422 to 680 MPa, the bond strength increased by 11.6%. This shows that the bond strength is reduced when the reinforcement yields [52]. When the rebar yields, the Poisson effect induces a radial contraction of the rebar, reducing the external pressure surrounding the rebar and causing a reduction in the bond strength [53]. However, with the yield strength of 680 MPa steel bars compared to 422 MPa steel bars, the post-peak toughness of A_{80} and A_{50} was 17.8% and 18.0% lower, respectively.

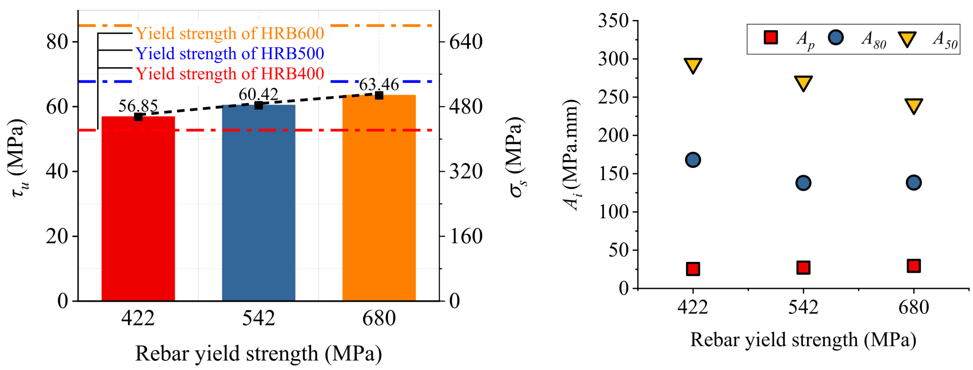

(**a**) (**b**)

Figure 12. Effect of rebar yield strength on bond performance: (**a**) bond strength; (**b**) bond toughness.

3.4.6. Loading Method and Debonded Length

The influence of the loading method and the debonded length on the bond property is shown in Figure 13. The formation of compression struts between the support and the surface of the reinforcing bar due to the support conditions, placing the surrounding concrete in compression [46]. The additional constraints increase the bond strength for the traditional pull-out test when the debonded length is less than the bond length (Figure 13a). The revised pull-out test bonded the reinforcement to the concrete at the loading surface, causing concrete spalling damage before the bars pull-out failure occurs [54], reducing the bond strength. UD-S02B-6D16C5-RP0 has 22.8% reduced bond strength compared to UD-S02B-6D16C5-P0.

When the debonded length was 40 mm ($2.5d_b$), the influence of the loading method on the bond strength was reduced to 6%. The effects of the loading methods on the bond strength were less than 1% when the debonded length was 84 mm ($5.25d_b$).

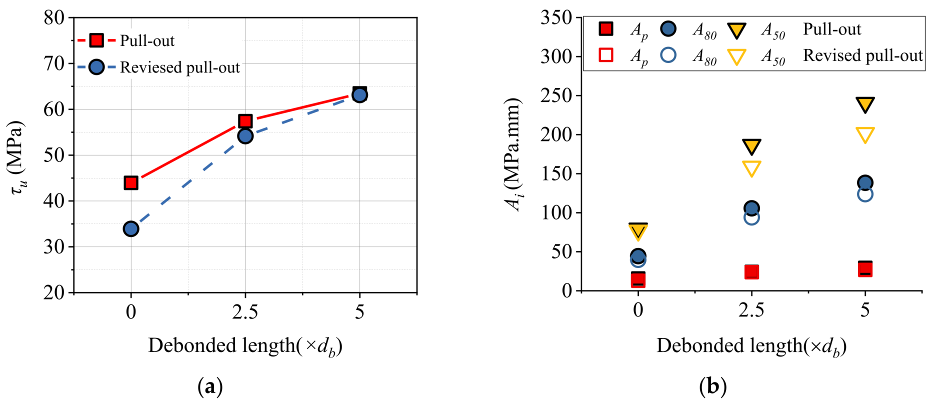

Figure 13. Effect of loading method and debonded length on bond performance: (**a**) bond strength; (**b**) bond toughness.

In conclusion, when the compressive force is applied to the loading surface at a distance larger than the bond length (32 mm) to the traditional pull-out test reinforcement, the desired stress state for the steel and the surrounding UHPC is close to simultaneously in tension [47]. The impact of the loading methods on the bond strength can be neglected.

The bond toughness of the traditional pull-out test specimens was more significant than the revised pull-out test specimens, as shown in Figure 13b. A_p, A_{80}, and A_{50} improved by 23.6%, 11.9%, and 3.5%, respectively, when the bonded part was located at the loading surface. A_p, A_{80}, and A_{50} improved by 2.2%, 12.3%, and 17.6%, respectively, when the debonded length was 40 mm. A_p, A_{80}, and A_{50} improved by 10.6%, 11.8%, and 19.1%, respectively, when the debonded length was 84 mm. According to the findings, the traditional pull-out test setup provided better energy-absorbing capabilities during the bond failure process than the revised pull-out test setup.

4. Analytical Model

4.1. Bond Strength Model

The existing bond strength models are reviewed, as listed in Table 7. The calculated results are compared with the experimental results [11,16,22,24,55,56], as shown in Figure 14. The existing models underestimate the actual bond strength.

Table 7. Summary of typical bond strength equations (SI units).

Type	Reference	Equations
NC	Orangun et al. [57]	$\tau_u = \sqrt{f_c{}'}[0.10 + 0.25(c/d_b) + 4.15(d_b/l_d) + (A_{sv}f_{sv}/41.5snd_b)]$
	AS3600 [58]	$\tau_u = 0.265\sqrt{f_c{}'}(c/d_b + 0.5)$
	CEB-FIP [35]	$\tau_u = 2.5\sqrt{f_c{}'}$
	Zuo and Darwin [59]	$\tau_u = f_c{}'^{1/4}(0.23 + 0.46c_{\min}/d_b + 14.05d_b/l_d)(0.1c_{\max}/c_{\min} + 0.9)$
UHPC	Marchand [13]	$\tau_u = 0.875\sqrt{f_c{}'}(c/d_b)\ c/d_b \leq 4$; $\tau_u = 3.9\sqrt{f_c{}'}\ c/d_b \geq 4$
	Roy [60]	$\tau_u = (0.45c/d_b + 38.5/l_d + 0.23V_f)f_t$
	Sturm [15]	$\tau_u = (0.0018c + 0.186)f_c{}'$

Note: $f_c{}'$: compressive strength of concrete cylinder; f_t: tensile strength of concrete; c: concrete cover; d_b: diameter of bar; l_d: embedment length; A_{sv}: area of transverse reinforcement; f_{sv}: yield strength of transverse reinforcement; s: spacing of transverse reinforcement; n: number of bars developed at the same location; $c_{\max}$, $c_{\min}$: maximum and minimum concrete cover.

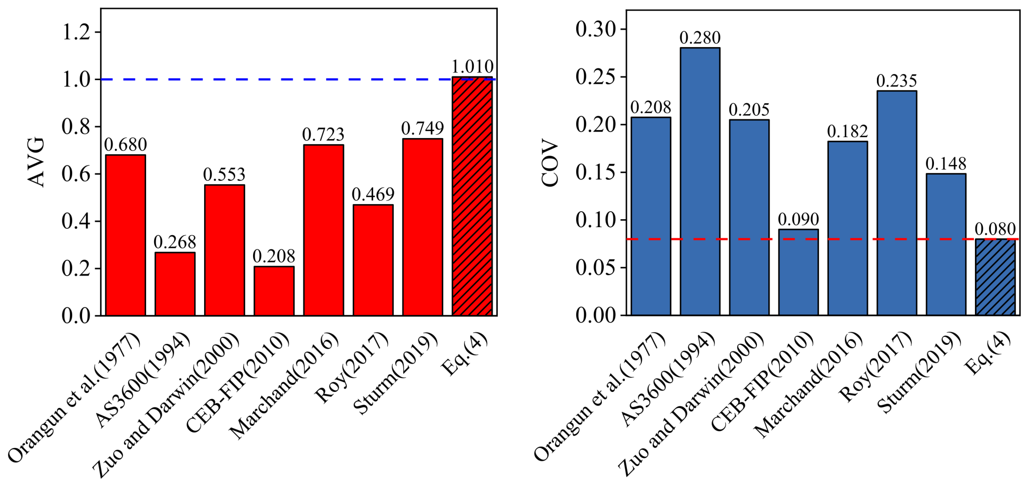

(**a**) (**b**)

Figure 14. Comparative the calculated bond strength of steel bar in UHPC: (**a**) the average ratio; (**b**) the coefficient of variation.

According to the test results and the existing formula, the main influencing factors are UHPC compressive strength f_c, cover thickness to rebar diameter ratio c/d_b, and fiber characteristic factor λ_f ($V_f \times L_f/d_f$). Using the least square method, we obtain the bond strength expression of rebar-UHPC as follows:

$$\tau_u = \sqrt{f_c}(0.13c/d_b + 0.47\lambda_f + 3.91) \tag{4}$$

The proposed formula fits well with the test results in this paper and the collected results from previous literature [11,16,22,24,55,56], as shown in Figure 15. The average ratio of the calculated value to the experimental value is 1.010. The coefficient of variation is 0.080.

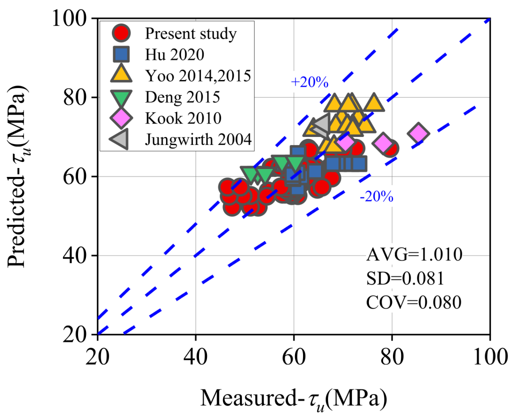

Figure 15. Comparative measured and predicted bond strength of UHPC.

4.2. Bond Stress-Slip Relationship Model

4.2.1. The Peak Slip s_u

According to the test results, the compressive strength, fiber content, and fiber type of UHPC have little influence on the peak slip. The cover thickness and rebar diameter are the significant factors affecting the peak slip. The expression for peak slip is obtained by regression analysis.

$$s_u = 0.04c/d_b + 0.0036{d_b}^2 - 0.569 \tag{5}$$

where s_u is the peak slip, c is the concrete cover thickness, d_b is the rebar diameter.

The calculated peak slips by Equation (5) are compared with the test results [9,11,24,56,61] in Figure 16. The average value and coefficient of variation of the predicted value to the test value are 1.006 and 0.185. Equation (5) provides suitable predictions.

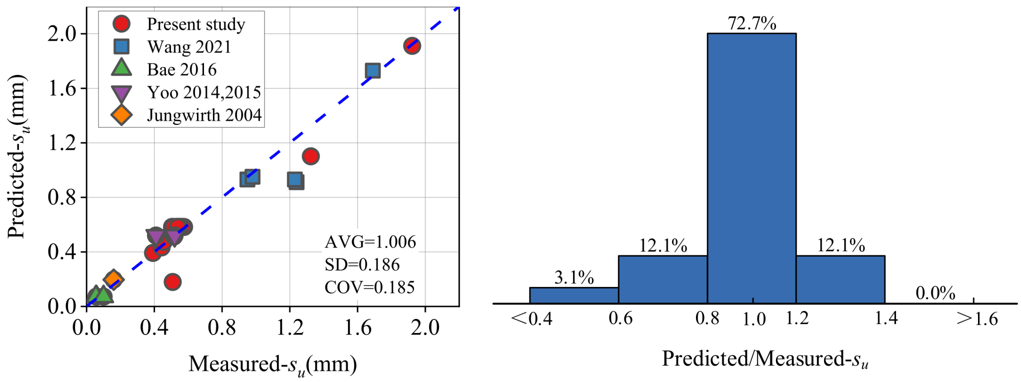

(**a**) (**b**)

Figure 16. Comparative measured and predicted results: (**a**) the peak slip s_u; (**b**) histogram.

4.2.2. Bond-Slip Relationship Model

According to the test results and the previous literature [11,15], a two-stage local bond stress-slip constitutive model of rebar-UHPC is proposed, which is in the form of an exponential function:

$$\text{Ascending}: \tau = \tau_u \left(1 - e^{-s/s_r}\right)^a \ s \leq s_u \tag{6}$$

$$\text{Descending}: \tau = \tau_u e^{-\beta(s - s_u)} \ s > s_u \tag{7}$$

where τ is the local bond stress, s is the relative slip between rebar and concrete, τ_u is the bond strength corresponding to the peak load, and s_u is the peak slip, which Equation (4) and Equation (5) determine, respectively. s_r, a, and β are obtained by regression analysis of experimental results.

The characteristic parameters of s_r, a, and β in the formula are determined as 0.112, 0.805, and 0.157, respectively, by the least square error method. The statistical results of fitting coefficients are listed in Table 8. The test results in this paper and performed by other researchers [11,24,62,63] are compared with analysis models, as shown in Figures 17 and 18, respectively. The proposed model can reasonably predict the bond stress-slip curve of rebar-UHPC.

Table 8. Statistical results of fitting coefficients.

Coefficient	Mean	Standard Deviation	Coefficient of Variation
s_r	0.112	0.034	0.301
α	0.805	0.178	0.221
β	0.157	0.029	0.183

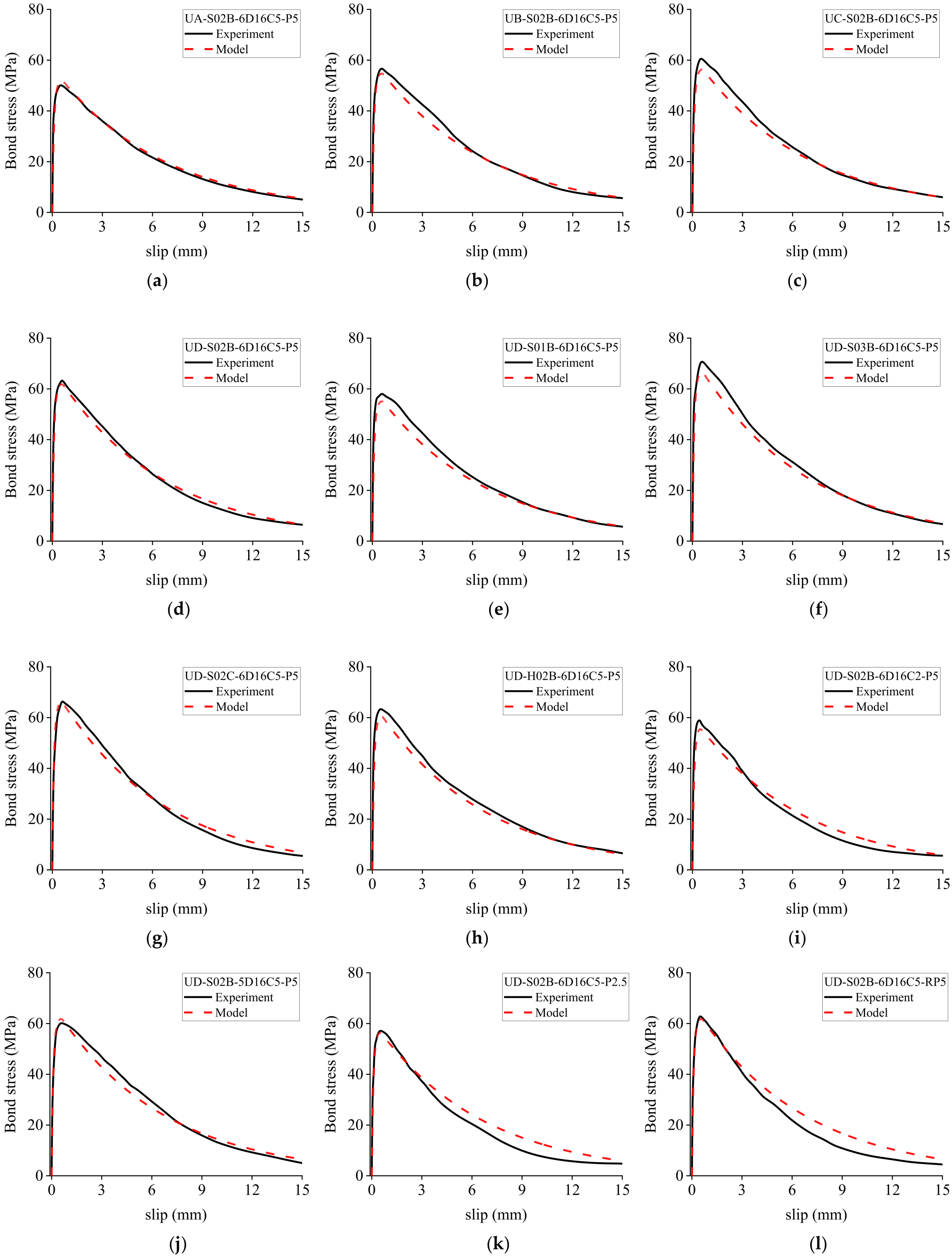

Figure 17. Comparison of the model predictions with the tested bond-slip curves: (**a**) UA-S02B-6D16C5-P5; (**b**) UB-S02B-6D16C5-P5; (**c**) UC-S02B-6D16C5-P5; (**d**) UD-S02B-6D16C5-P5; (**e**) UD-S01B-6D16C5-P5; (**f**) UD-S03B-6D16C5-P5; (**g**) UD-S02C-6D16C5-P5; (**h**) UD-H02B-6D16C5-P5; (**i**) UD-S02B-6D16C2-P5; (**j**) UD-S02B-5D16C5-P5; (**k**) UD-S02B-6D16C5-P2.5; (**l**) UD-S02B-6D16C5-RP5.

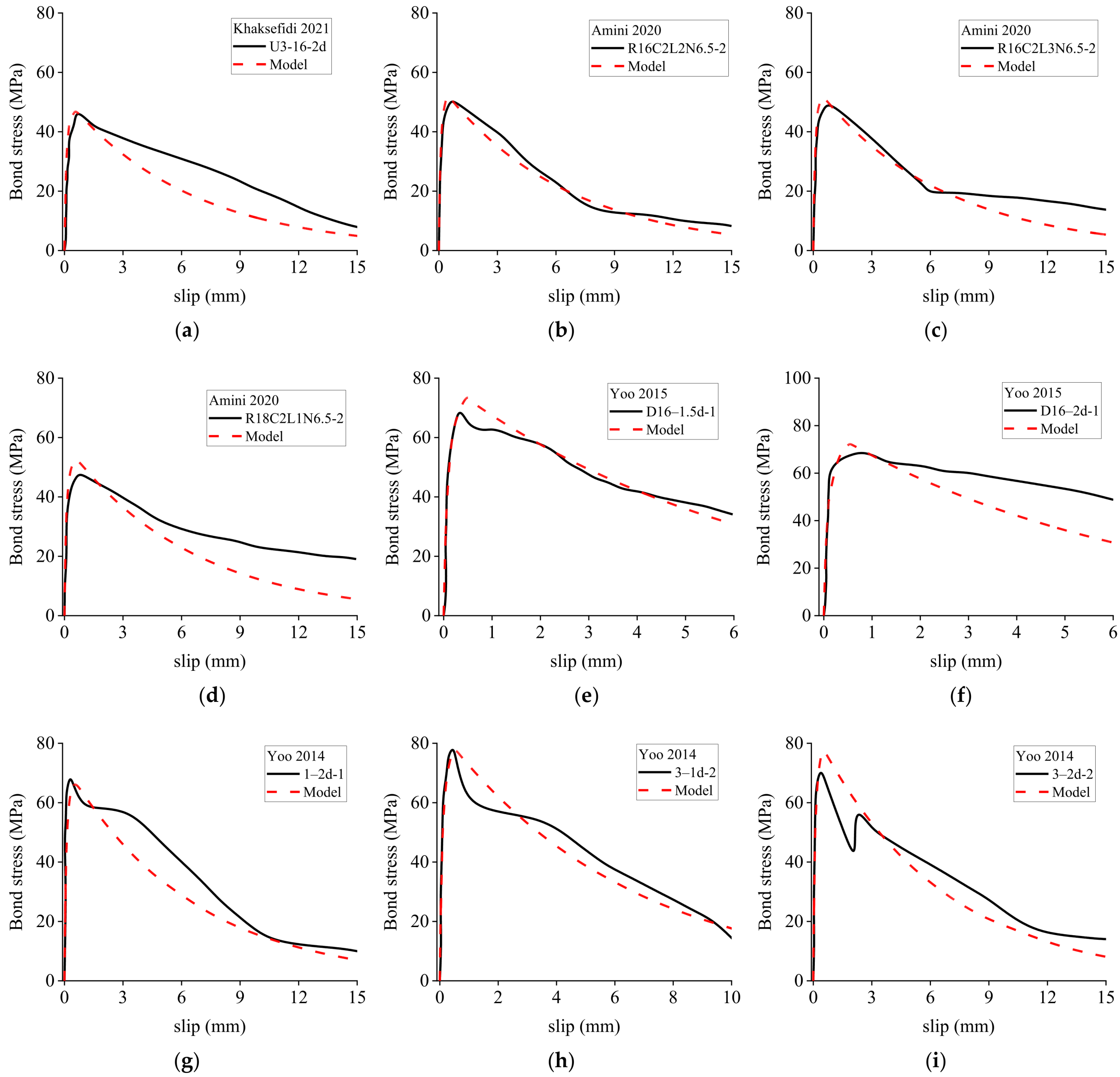

Figure 18. Comparison of the model predictions with the tested bond-slip curves by other researchers: (**a**) U3-16-2d; (**b**) R16C2L2N6.5-2; (**c**) R16C2L3N6.5-2; (**d**) R18C2L1N6.5-2; (**e**) D16-1.5d-1; (**f**) D16-2d-1; (**g**) 1-2d-1; (**h**) 3-1d-2; (**i**) 3-2d-2.

5. Conclusions

Sixty-nine rebar-UHPC pull-out specimens were designed and tested under monotonic loading. The variables include UHPC compressive strength, steel fiber volume content, steel fiber types, cover thickness, rebar diameter, yield strength, loading method, and the debonded length. Based on the results and discussions above, the main conclusions are as follows:

(1) The UHPC effectively increases the bond strength of the rebars. The bond strength is linearly related to the square root of UHPC compressive strength in MPa;

(2) Increasing the fiber volume content and aspect ratio can increase the bond strength. A fiber characteristic factor λ_f ($\lambda_f = V_f \times L_f/d_f$) is used to evaluate the effects of fiber volume content and aspect ratio. The bond strength of the specimens with the hook steel fiber has no significant difference from the straight steel fiber;

(3) As the cover thickness increases from $1d_b$ to $2d_b$, the bond strength increases by 17.6%. The bond strength remains unchanged when the cover thickness is greater than $2d_b$. The peak slip increases by 43.6% when the cover thickness changes from $1d_b$ to $5.75d_b$;
(4) The influence of rebar diameter on bond strength is negligible since bond strength remains almost constant as rebar diameter increases. When the rebar diameter raises from 12 to 25 mm, the peak slips improve by 276.4%. The bond strength increases with the rebar grade;
(5) The impact of the loading methods on the bond strength can be neglected when the debonded length is greater than the bond length;
(6) A simplified bond strength formula is suggested, fitting well with the test results in this paper and the collected results from previous literature. The average ratio of the calculated value to the experimental value is 1.010, with the coefficient of variation being 0.080. The peak slip expression is developed for the rebar-UHPC interface, which has significant consequences for cover thickness and rebar diameter;
(7) A two-branch bond stress-slip constitutive model is proposed to describe the bond behavior of rebar in UHPC. The predicted bond-slip curves are in suitable agreement with the test curves.

Author Contributions: Methodology, R.L. and Y.H.; data curation, investigation and writing—original draft, R.L.; writing—review and editing, Y.H. and Z.X.; funding acquisition, Y.H. All authors have read and agreed to the published version of the manuscript.

Funding: This research was funded by the National Natural Science Foundation of China (no. 51890901) and the Natural Science Foundation for Distinguished Young Scholars of Hunan Province, China (no. 2020JJ2003).

Institutional Review Board Statement: Not applicable.

Informed Consent Statement: Not applicable.

Data Availability Statement: The data presented in this study are available on request from the corresponding author.

Conflicts of Interest: The authors declare no conflict of interest.

References

1. Shafieifar, M.; Farzad, M.; Azizinamini, A. Experimental and numerical study on mechanical properties of Ultra High Performance Concrete (UHPC). *Constr. Build. Mater.* **2017**, *156*, 402–411. [CrossRef]
2. Zhang, Y.; Yang, J.; Li, T.; Deng, M. Mechanical behavior of RC columns strengthened with thin UHPC jacket under cyclic loads. *J. Build. Eng.* **2022**, *49*, 104065. [CrossRef]
3. Wang, Y.; Shao, X.; Chen, J.; Cao, J.; Deng, S. UHPC-based strengthening technique for orthotropic steel decks with significant fatigue cracking issues. *J. Constr. Steel Res.* **2021**, *176*, 106393. [CrossRef]
4. Graybeal, B.; Crane, C.K.; Perry, V.; Corvez, D.; Ahlborn, T.M. Advancing Ultra-High-Performance Concrete. *Concr. Int.* **2019**, *41*, 41–45.
5. Kim, J.J.; Yoo, D.Y. Effects of fiber shape and distance on the pullout behavior of steel fibers embedded in ultra-high-performance concrete. *Cem. Concr. Compos.* **2019**, *103*, 213–223. [CrossRef]
6. Fan, L.; Meng, W.; Teng, L.; Khayat, K.H. Effects of lightweight sand and steel fiber contents on the corrosion performance of steel rebar embedded in UHPC. *Constr. Build. Mater.* **2020**, *238*, 117709. [CrossRef]
7. El-Joukhadar, N.; Pantazopoulou, S.J. Effectiveness of UHPFRC cover in delaying bar corrosion. *Constr. Build. Mater.* **2021**, *269*, 121288. [CrossRef]
8. Ma, F.; Deng, M.; Ma, Y.; Lue, H.; Yang, Y.; Sun, H. Experimental study on interior precast concrete beam-column connections with lap-spliced steel bars in field-cast RPC. *Eng. Struct.* **2021**, *228*, 111481. [CrossRef]
9. Bae, B.I.; Choi, H.K.; Choi, C.S. Bond stress between conventional reinforcement and steel fibre reinforced reactive powder concrete. *Constr. Build. Mater.* **2016**, *112*, 825–835. [CrossRef]
10. Holschemacher, K.; Weiße, D.; Klotz, S. Bond of reinforcement in ultra high strength concrete. In Proceedings of the International Symposium on Ultra High Performance Concrete, Kassel, Germany, 13–15 September 2004; pp. 375–387.
11. Yoo, D.Y.; Shin, H.O.; Yang, J.M.; Yoon, Y.S. Material and bond properties of ultra high performance fiber reinforced concrete with micro steel fibers. *Compos. Part B* **2014**, *58*, 122–133. [CrossRef]

12. Fehling, E.; Lorenz, P.; Leutbecher, T. Experimental Investigations on Anchorage of Rebars in UHPC. In Proceedings of the Hipermat 2012 3rd International Symposium on UHPC and Nanotechnology for High Performance Construction Materials, Kassel, Germany, 7–9 March 2012; pp. 533–540.
13. Marchand, P.; Baby, F.; Khadour, A.; Battesti, T.; Rivillon, P.; Quiertant, M.; Nguyen, H.H.; Généreux, G.; Deveaud, J.P.; Simon, A. Bond behaviour of reinforcing bars in UHPFRC. *Mater. Struct.* **2016**, *49*, 1979–1995. [CrossRef]
14. Alkaysi, M.; El-Tawil, S. Factors affecting bond development between Ultra High Performance Concrete (UHPC) and steel bar reinforcement. *Constr. Build. Mater.* **2017**, *144*, 412–422. [CrossRef]
15. Sturm, A.B.; Visintin, P. Local bond slip behavior of steel reinforcing bars embedded in ultra high performance fibre reinforced concrete. *Struct. Concr.* **2019**, *20*, 108–122. [CrossRef]
16. Hu, A.X.; Liang, X.W.; Shi, Q.X. Bond Characteristics between High-Strength Bars and Ultrahigh-Performance Concrete. *J. Mater. Civ. Eng.* **2020**, *32*, 1–14. [CrossRef]
17. Lee, J.Y.; Lim, A.R.; Kim, J.; Kim, J. Bond behaviour of GFRP bars in high-strength concrete: Bar diameter effect. *Mag. Concr. Res.* **2017**, *69*, 541–554. [CrossRef]
18. Metelli, G.; Plizzari, G.A. Influence of the relative rib area on bond behaviour. *Mag. Concr. Res.* **2014**, *66*, 277–294. [CrossRef]
19. Bamonte, P.F.; Gambarova, P.G. High-bond bars in NSC and HPC: Study on size effect and on the local bond stress-slip law. *J. Struct. Eng.* **2007**, *133*, 225–234. [CrossRef]
20. Bazant, Z.P.; Sener, S. Size effect in pull-out tests. *ACI Mater. J.* **1988**, *85*, 347–351.
21. Seo, J.; Lee, G.C.; Liang, Z.; Dargush, G.F. Configuration and Size Effects on Bond Stress-Slip and Failure Modes of RC Connections. *J. Eng. Mech.* **2014**, *140*, 04014082. [CrossRef]
22. Kook, K.H.; Shin, H.O.; Kwahk, I.J.; Yoon, Y.S. Bond Characteristics of Ultra High Performance Concrete. *J. Korea Concr. Inst.* **2010**, *22*, 753–760. [CrossRef]
23. Lagier, F.; Massicotte, B.; Charron, J.P. Bond strength of tension lap splice specimens in UHPFRC. *Constr. Build. Mater.* **2015**, *93*, 84–94. [CrossRef]
24. Yoo, D.Y.; Kwon, K.Y.; Park, J.J.; Yoon, Y.S. Local bond-slip response of GFRP rebar in ultra-high-performance fiber-reinforced concrete. *Compos. Struct.* **2015**, *120*, 53–64. [CrossRef]
25. Yuan, J.; Graybeal, B.A. *Bond Behavior of Reinforcing Steel in Ultra-High Performance Concrete*; US Department of Transportation, Federal Hifhway Administartion: McLean, VA, USA, 2014.
26. Firas, S.A.; Gilles, F.; Robert, L. Bond between carbon fibre-reinforced polymer (CFRP) bars and ultra high performance fibre reinforced concrete (UHPFRC): Experimental study. *Constr. Build. Mater.* **2011**, *25*, 479–485. [CrossRef]
27. Lin, H.W.; Zhao, Y.X.; Ozbolt, J.; Feng, P.; Jiang, C.; Eligehausen, R. Analytical model for the bond stress-slip relationship of deformed bars in normal strength concrete. *Constr. Build. Mater.* **2019**, *198*, 570–586. [CrossRef]
28. Delso, J.M.; Stavridis, A.; Shing, P. Bond Strength and Cyclic Bond Deterioration of Large-Diameter Bars. *ACI Struct. J.* **2013**, *110*, 659–670.
29. Chao, S.-H.; Naaman, A.E.; Parra-Montesinos, G.J. Local Bond Stress-Slip Models for Reinforcing Bars and Prestressing Strands in High-Peformance Fiber-Reinforced Cement Composites. *ACI Special Publication* **2010**, *272*, 151–172.
30. Wu, Y.F.; Zhao, X.M. Unified Bond Stress-Slip Model for Reinforced Concrete. *J. Struct. Eng.* **2013**, *139*, 1951–1962. [CrossRef]
31. Xu, Y.L. *Experimental Study of Anchorage Properties for Deformed Bars in Concrete; Tsinghua University: Beijing, China, 1990. (In Chinese)*
32. Zhao, W.P.; Zhu, B.R. Theoretical model for the bond-slip relationship between ribbed steel bars and confined concrete. *Struct. Concr.* **2018**, *19*, 548–558. [CrossRef]
33. Lee, Y.H.; Joo, Y.T.; Lee, T.; Ha, D.H. Mechanical properties of constitutive parameters in steel–concrete interface. *Eng. Struct.* **2011**, *33*, 1277–1290. [CrossRef]
34. Chao, S.-H. Bond Characterization Of Reinforcing Bars and Prestressing Strands in High Performance Fiber Reinforced Cementitious Composites under Monotonic and Cyclic Loading. Ph.D. Thesis, University of Michigan, Ann Arbor, MI, USA, 2005.
35. CEB-FIP. *Fib Model Code for Concrete Structures 2010*; Comité Euro international du Béton/Federation Internationale de la Precontrainte: Lausanne, Switzerland, 2013.
36. *GB 50010-2010*; Code for Design of Concrete Structures. China Architecture & Building Press: Beijing, China, 2015.
37. Harajli, M.H.; Hamad, B.S.; Rteil, A.A. Effect of confinement of bond strength between steel bars and concrete. *ACI Struct. J.* **2004**, *101*, 595–603.
38. Huang, L.; Chi, Y.; Xu, L.; Chen, P.; Zhang, A. Local bond performance of rebar embedded in steel-polypropylene hybrid fiber reinforced concrete under monotonic and cyclic loading. *Constr. Build. Mater.* **2016**, *103*, 77–92. [CrossRef]
39. Gao, X.L.; Li, N.K.; Ren, X.D. Analytic solution for the bond stress-slip relationship between rebar and concrete. *Constr. Build. Mater.* **2019**, *197*, 385–397. [CrossRef]
40. Bravo, M.; Duarte, A.P.C.; de Brito, J.; Evangelista, L. Tests and Simulation of the Bond-Slip between Steel and Concrete with Recycled Aggregates from CDW. *Buildings* **2021**, *11*, 40. [CrossRef]
41. Zhou, Z.D.; Qiao, P.Z. Bond behavior of epoxy-coated rebar in ultra-high performance concrete. *Constr. Build. Mater.* **2018**, *182*, 406–417. [CrossRef]
42. *GB/T 31387-2015*; Reactive Powder Concrete. China Standard Press: Beijing, China, 2015.
43. Li, W.; Huang, Z.; Hu, G.; Hui Duan, W.; Shah, S.P. Early-age shrinkage development of ultra-high-performance concrete under heat curing treatment. *Constr. Build. Mater.* **2017**, *131*, 767–774. [CrossRef]

44. *GB/T 1499.2-2018*; Steel for the Reinforcement of Concrete-Part 2: Hot Rolled Ribbed Bars. China Standard Press: Beijing, China, 2018.
45. RILEM TC. RC6: Bond Test for Reinforcement Steel: 2: Pull-Out Test, 1983. In *RILEM Recommendations for the Testing and Use of Construction Materials*; E & FN SPON: London, UK, 1994; pp. 218–220.
46. Saikali, E.R. Bond Behaviour of Steel Reinforcing Bars Embedded in Ultra-High-Performance Steel Fiber Reinforced Concrete. Master's Thesis, York University, Toronto, ON, Canada, 2019.
47. ACI Committee 408. *ACI 408R-03: Bond and Development of Straight Reinforcing Bars in Tension*; American Concrete Institute: Farmington Hills, MI, USA, 2003.
48. Yao, Y.; Zhang, H.; Zhang, X.; Ren, F.; Li, Y.; Yang, Z. Experimental, Analytical and Numerical Studies of Interfacial Bonding Properties between Silane-Coated Steel Fibres and Mortar. *Buildings* **2021**, *11*, 398. [CrossRef]
49. Harajli, M.H.; Mabsout, M.E. Evaluation of Bond Strength of Steel Reinforcing Bars in Plain and Fiber-Reinforced Concrete. *ACI Struct. J.* **2002**, *99*, 509–517.
50. Zhao, M.; Liu, G.; Liu, L.; Zhang, Y.; Shi, K.; Zhao, S. Bond of Ribbed Steel Bar in High-Performance Steel Fiber Reinforced Expanded-Shale Lightweight Concrete. *Buildings* **2021**, *11*, 582. [CrossRef]
51. Qi, J.; Cheng, Z.; John Ma, Z.; Wang, J.; Liu, J. Bond strength of reinforcing bars in ultra-high performance concrete: Experimental study and fiber–matrix discrete model. *Eng. Struct.* **2021**, *248*, 113290. [CrossRef]
52. Bonacci, J.F. Bar Yield Penetration in Monotonically Loaded Anchorages. *J. Struct. Eng.* **1994**, *120*, 965–986. [CrossRef]
53. Ma, F.; Deng, M.; Fan, H.; Yang, Y.; Sun, H. Study on the lap-splice behavior of post-yield deformed steel bars in ultra high performance concrete. *Constr. Build. Mater.* **2020**, *262*, 120611. [CrossRef]
54. Chu, S.H.; Kwan, A.K.H. A new method for pull out test of reinforcing bars in plain and fibre reinforced concrete. *Eng. Struct.* **2018**, *164*, 82–91. [CrossRef]
55. Deng, Z.C.; Cheng, S.K. HRB 500 high-strength reinforced and reactive power concrete bond-slip constitutive relations research. *Concrete* **2015**, *303*, 25–31. (In Chinese)
56. Jungwirth, J.; Muttoni, A. Structural behavior of tension members in Ultra High Performance Concrete. In Proceedings of the International Symposium on Ultra High Performance Concrete, Kassel, Germany, 13–15 September 2004.
57. Orangun, C.; Jirsa, J.O.; Breen, J. *The Strength of Anchor Bars: A Reevaluation of Test Data on Development Length and Splices*; University of Texas: Austin, Texas, USA, 1975.
58. *AS3600*; Australian Standard for Concrete Structures. Standards Australia Limited: Sydney, Australia, 1994.
59. Zuo, J.; Darwin, D. Bond slip of high relative rib area bars under cyclic loading. *ACI Struct. J.* **2000**, *97*, 331–334.
60. Roy, M.; Hollmann, C.; Wille, K. Influence of volume fraction and orientation of fibers on the pullout behavior of reinforcement bar embedded in ultra high performance concrete. *Constr. Build. Mater.* **2017**, *146*, 582–593. [CrossRef]
61. Wang, D.; Han, L.; Ju, Y.; Zeng, C.; Li, Z. Bond behavior between reinforcing bar and reactive powder concrete. *Struct. Concr.* **2021**, 1–13. [CrossRef]
62. Khaksefidi, S.; Ghalehnovi, M.; de Brito, J. Bond behaviour of high-strength steel rebars in normal (NSC) and ultra-high performance concrete (UHPC). *J. Build. Eng.* **2021**, *33*, 101592. [CrossRef]
63. Amini Pishro, A.; Feng, X.; Ping, Y.; Dengshi, H.; Shirazinejad, R.S. Comprehensive equation of local bond stress between UHPC and reinforcing steel bars. *Constr. Build. Mater.* **2020**, *262*, 119942. [CrossRef]